



The structure and evolution of lower stratospheric frontal zones. Part II: The influence of tropospheric ascent on lower stratospheric frontal development

Andrea A. Lang and Jonathan E. Martin*

Department of Atmospheric and Oceanic Sciences, University of Wisconsin – Madison, WI, USA

*Correspondence to: J. E. Martin, Department of Atmospheric and Oceanic Sciences, University of Wisconsin–Madison, 1225 W. Dayton Street, Madison, WI 53706, USA. E-mail: jemarti1@wisc.edu

The intensification of frontal characteristics in the region above the mid-latitude jet core within the lower stratospheric portion of an upper-level jet front system (ULJF) is known as lower stratospheric frontogenesis. Four recent cases of lower stratospheric frontogenesis in southwesterly flow are examined in order to elucidate the interaction between lower stratospheric dynamical processes and tropospheric ascent that characterizes such developments. In all of the cases examined the lower stratospheric front was (1) characterized by lower stratospheric quasi-geostrophic forcing for ascent on its cold side, and (2) parallel to a surface cold front.

As latent heating associated with ascent along the surface cold front redistributed the potential temperature field within the upper troposphere, the stability of the near-tropopause upper troposphere decreased, thus intensifying the response to lower stratospheric frontal forcing by enhancing the frontogenetic ascent within the upper troposphere. It is therefore suggested that ascent originating in the lower troposphere is able to influence the development of lower stratospheric fronts and substantially alter the structure of the mid-latitude tropopause and its associated horizontal potential vorticity gradient at and above the jet core. The implications of lower stratospheric frontogenetic processes on facilitating tropical–extratropical interactions is discussed.

Key Words: lower stratospheric fronts; convection; stability reduction

Received 2 August 2011; Revised 21 June 2012; Accepted 11 October 2012; Published online in Wiley Online Library 7 January 2013

Citation: AA Lang and JE Martin. 2013. The structure and evolution of lower stratospheric frontal zones. Part II: The influence of tropospheric ascent on lower stratospheric frontal development. *Q. J. R. Meteorol. Soc.* **139**: 1798–1809. DOI:10.1002/qj.2074

1. Introduction

A mid-latitude upper-level jet-front system (ULJF) consists of three component parts: (1) a jet core and attendant frontal structures in (2) the upper troposphere and (3) the lower stratosphere, associated (via thermal wind) with the vertical shear in those locations (Figure 1). The recent analysis by Lang and Martin (2012, hereafter Part I) demonstrates that consideration of the separate evolution of the lower stratospheric front (labelled 'LSF' in Figure 1) and upper tropospheric front (labelled 'UTF' in Figure 1) is necessary in order to fully understand the comprehensive life cycle

of a ULJF within a baroclinic wave. Upon the examination of two cases, the Part I analysis shows that while they have common governing dynamics, namely tilting frontogenesis, the upper tropospheric and lower stratospheric fronts develop asynchronously within the evolution of an ULJF through the northwesterly and southwesterly flow portions of a baroclinic wave. For a review of the background literature related to ULJFs and their attendant frontal structures the reader is directed to section 1 of Part I.

The dynamical underpinning of the analyses presented in Part I stems from prior work on upper tropospheric

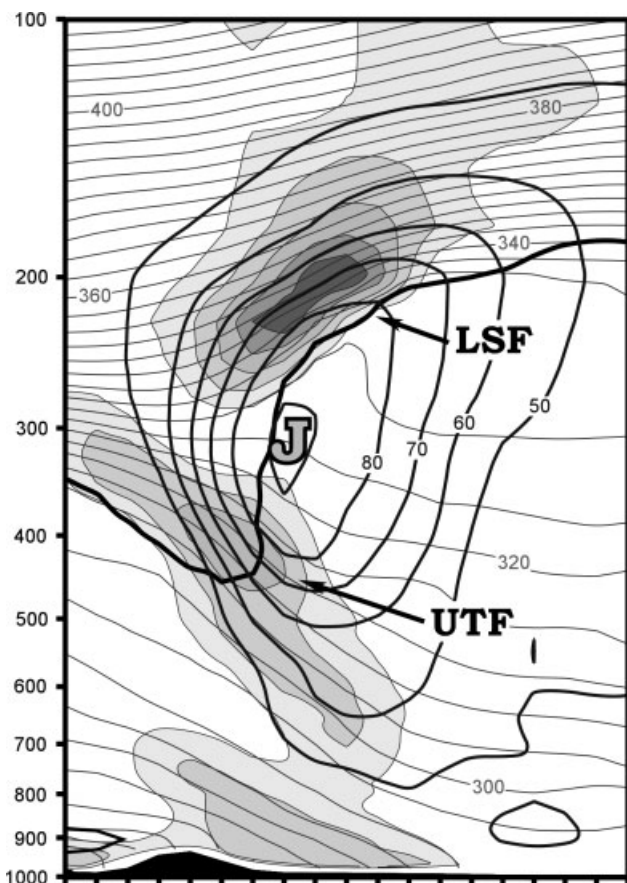


Figure 1. Cross-section the North Atlantic jet off the east coast of North America at 1200 UTC 27 February 2008, highlighting the jet core (marked with a 'J') and associated frontal structures. The upper tropospheric front is labelled 'UTF' and the lower stratospheric front is labelled 'LSF.' Isotachs are thick lines every 10 m s^{-1} beginning at 40 m s^{-1} , isentropes are thin lines every 4 K , and the magnitude of the horizontal potential temperature gradient is filled every $1 \text{ K (100 km)}^{-1}$ beginning at $2 \text{ K (100 km)}^{-1}$.

jet circulations (e.g. Shapiro, 1982; Rottuno *et al.*, 1994; Schultz and Doswell, 1999) and the fact that geostrophic temperature advection in the cyclonic shear portion of the ULJF produces favourable conditions for quasi-geostrophic (QG) vertical motion in the vicinity of the jet core. The Part I analysis highlights instances when the maximum geostrophic temperature advection was centred within the lower stratospheric portion of a ULJF and was tied to Sawyer (1956)–Eliassen (1962) type circulations above the level of maximum winds, in the vicinity of the lower stratospheric front. In northwesterly flow, geostrophic cold air advection in the lower stratospheric cyclonic shear was associated with subsidence through the local jet core that weakened an initially intense lower stratospheric front, via tilting (conceptualized in Figure 2(a)). The lower stratospheric frontolysis was also associated with a decrease in the slope of the tropopause above the jet core. This weakening of the lower stratospheric front occurred in concert with the development of an intense upper tropospheric front that provided a precursor disturbance for a substantial surface cyclogenesis event. In the southwesterly flow case, geostrophic warm air advection in lower stratospheric cyclonic shear promoted ascent on the cold side of the lower stratospheric front. This vertical motion in the near-tropopause region resulted in frontogenetic tilting, associated with both an enhancement of the frontal characteristics (e.g. cyclonic shear, static

stability, temperature gradient) and an increased slope of the tropopause, above the jet core (conceptualized in Figure 2(b)). Lang and Martin (2012) hypothesized that lower stratospheric frontogenetic processes can lead to substantial changes in the structure of the ULJF within which a lower stratospheric front is embedded. In addition, they noted that any changes to the mid-latitude ULJF structure and tropopause slope can have potential consequences on the downstream development of sensible weather systems.

A leading characteristic of the southwesterly flow case presented in Part I was the vertical superposition of two distinct ascent maxima centred in (1) the near-tropopause upper troposphere, in association with lower stratospheric QG forcing, and (2) in the lower troposphere, in association with frontogenetic forcing along a surface cold front. That analysis suggested that when a surface cold front and a lower stratospheric front become nearly vertically aligned (common in southwesterly flow), the latent heating accompanying the frontal ascent at the surface boundary can diabatically reduce the static stability of the upper troposphere. The reduced static stability can thereby encourage a robust response to frontogenetical forcing for ascent in the vicinity of the lower stratospheric front. The present paper examines this hypothesis from a case study perspective by considering the development of four robust southwesterly-flow lower stratospheric fronts and the influence on the lower stratospheric frontogenesis process that arises from coincident lower tropospheric ascent and associated latent heat release.

The paper is structured in the following manner. Section 2 provides an overview of each of the lower stratospheric front cases. The analysis of the four cases begins in Section 3, with an overview of the common mechanisms associated with the development of the robust lower stratospheric fronts. Section 4 provides a cross-sectional analysis of a representative sample of the cases, followed by a summary and discussion of the results highlighted in section 5.

2. Case overviews

In order to investigate the lower tropospheric connection to robust cases of lower stratospheric frontogenesis in southwesterly flow, the present work highlights four ULJFs observed during the winter of 2008–2009 off of the east coast of North America. During that winter season, specifically the period November 2008 to March 2009, the lower stratospheric and upper tropospheric frontal characteristics were documented and archived using data from twice-daily (0000 and 1200 UTC) analyses (00 h forecasts) from the $0.5^\circ \times 0.5^\circ$ grid of the National Center for Environmental Prediction's (NCEP) Global Forecast System (GFS) model. From this archive four events were selected to represent a sample of the strongest lower stratospheric front cases, each possessing a 200 hPa potential temperature gradient magnitude ($|\nabla\theta|$) exceeding $8 \text{ K (100 km)}^{-1}$ during the most intense phase of their life cycles in southwesterly flow.

Employing the GFS gridded model analyses, the following section provides a brief overview of the evolution of the lower stratospheric and upper tropospheric fronts in each of these ULJF cases. The evolution the 200 hPa $|\nabla\theta|$ will be used to represent the lower stratospheric front as 200 hPa was consistently located above the level of maximum winds of the southwesterly flow polar jet. The $|\nabla\theta|$ of the corresponding upper tropospheric frontal

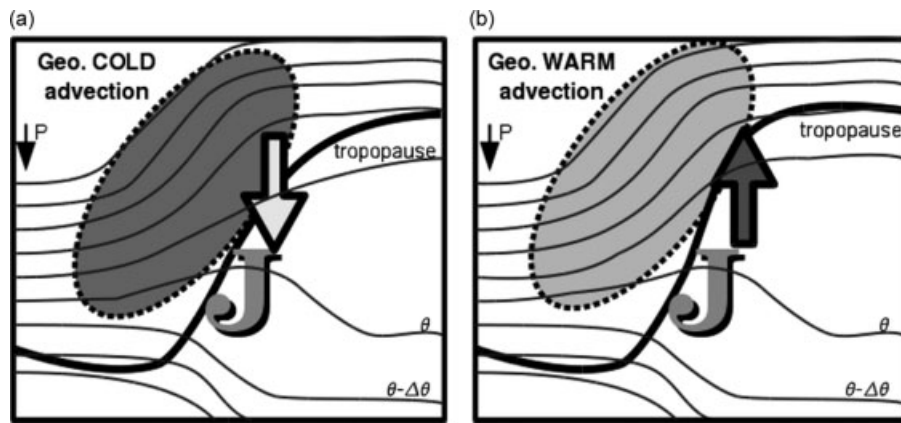


Figure 2. Conceptual models of lower stratospheric frontolysis in (a) northwesterly flow and (b) southwesterly flow, as summarized in the text: (a) with geostrophic cold air advection (shaded), subsidence represented by the arrow, idealized potential temperature (thin line) and jet core represented by 'J'; (b) as in (a) but with geostrophic warm air advection shaded and ascent represented by the arrow.

structure is shown at 500 hPa, a level below the jet core and consistent with previous literature on upper tropospheric frontal dynamics (e.g. Keyser and Shapiro, 1986). Each of the overviews presented here corresponds to a period of lower stratospheric frontogenesis that lasted at least 12 h. Two times within the evolution are highlighted: one 12 h prior to ($T = T_o - 12$ h), and a second at the time of ($T = T_o$), the maximum intensity of each lower stratospheric front. These four cases (where T_o equals 0600 UTC 20 November 2008, 1200 UTC 8 December 2008, 1800 UTC 7 January 2009 and 1800 UTC 4 March 2009) are representative samples of cases that occurred throughout the winter season. In addition, this section provides a brief overview of the lower tropospheric synoptic environment for each case at T_o . The 950 hPa horizontal frontogenesis will be used to illustrate the forcing for lower tropospheric ascent in each case.

2.1. Evolution at 200 hPa

Figure 3 highlights the evolution of the four robust lower stratospheric fronts at 200 hPa. Each of the lower stratospheric fronts was situated within southwesterly flow between a high-amplitude trough–ridge couplet in the vicinity of the east coast of North America. For each of the four cases, the region of enhanced $|\nabla\theta|$ that characterized the lower stratospheric front accounted for the majority of the 30 K difference between the lower stratospheric potential temperature within the trough (~ 360 K) and the colder upper tropospheric air in the downstream ridge (~ 330 K). During the 12 h period of the analysis, each of the synoptic scale troughs acquired a more negative tilt, regardless of whether the corresponding troughs began the period of investigation with a negative tilt (e.g. Case 1, Figure 3(a, b), and Case 2, Figure 3(c, d)) or an initially positive tilt that weakened (e.g. Case 3, Figure 3(e, f)). In addition, the half wavelength between the upstream trough and downstream ridge shortened over these periods of lower stratospheric frontogenesis. As the amplitude of the mid-latitude flow increased at 200 hPa, the lower stratospheric fronts intensified (Figure 3), with the most notable increase in $|\nabla\theta|$ occurring in Case 4 (Figure 3(g, h)), where $|\nabla\theta|$ increased from $5 \text{ K (100 km)}^{-1}$ to $8 \text{ K (100 km)}^{-1}$. Although $|\nabla\theta|$ in Case 3 (Figure 3(e, f)) remained relatively constant, the geographic extent of the lower stratospheric front increased substantially over the

12 h period. Such an increase of the geographic extent of the lower stratospheric front was a characteristic of all the cases. By T_o , a robust lower stratospheric front exceeding $8 \text{ K (100 km)}^{-1}$ was present in all four cases.

2.2. Evolution at 500 hPa

The evolution of the 500 hPa flow and corresponding upper tropospheric fronts is shown in Figure 4. During this period, the southerly component of the flow between the upstream trough and downstream ridge increased as the synoptic pattern amplified. In each case, the orientation of the geopotential height at 500 hPa (Figure 4) and 200 hPa (Figure 3) at both $T_o - 12$ h and T_o suggested that the geostrophic wind veered with height consistent with geostrophic warm air advection in the layer (discussed further in section 3.2). Within the southwesterly flow, the regions of enhanced $|\nabla\theta|$ that corresponded to the upper tropospheric fronts were less coherent and less robust than their lower stratospheric counterparts. Cases 1, 2 and 4 (Figure 4(a, b), (c, d) and (g, h), respectively) exhibited multiple regions of enhanced $|\nabla\theta|$ at both times and experienced either a weakening or maintenance of the $|\nabla\theta|$ over the 12 h period. The $|\nabla\theta|$ in Case 3 (Figure 4(e, f)) was of comparable magnitude to the corresponding lower stratospheric front at $T_o - 12$ h but weakened with time and covered a smaller geographic area than its companion in the lower stratosphere at T_o . By T_o , both the geographic extent and intensity of all four of the upper tropospheric fronts were subordinate to their lower stratospheric counterparts.

2.3. Lower troposphere analysis

The lower tropospheric analysis at T_o is shown in Figure 5 for the four cases. A sea-level pressure (SLP) minimum between ~ 975 hPa and ~ 1005 hPa was present in each case. Extending to the north and east of each SLP minimum was a warm front denoted at 950 hPa by an enhanced equivalent potential temperature (θ_e) gradient and a region of horizontal frontogenesis. In all four cases, the cold front and the frontogenesis associated with the cold front were south and east of the cyclone centre. The thermal structure of the cases suggested that these cyclones were in the mature to occluded stages of their life cycles. Upon closer investigation, the thermal structure of two of the cases, Cases 2 and 3

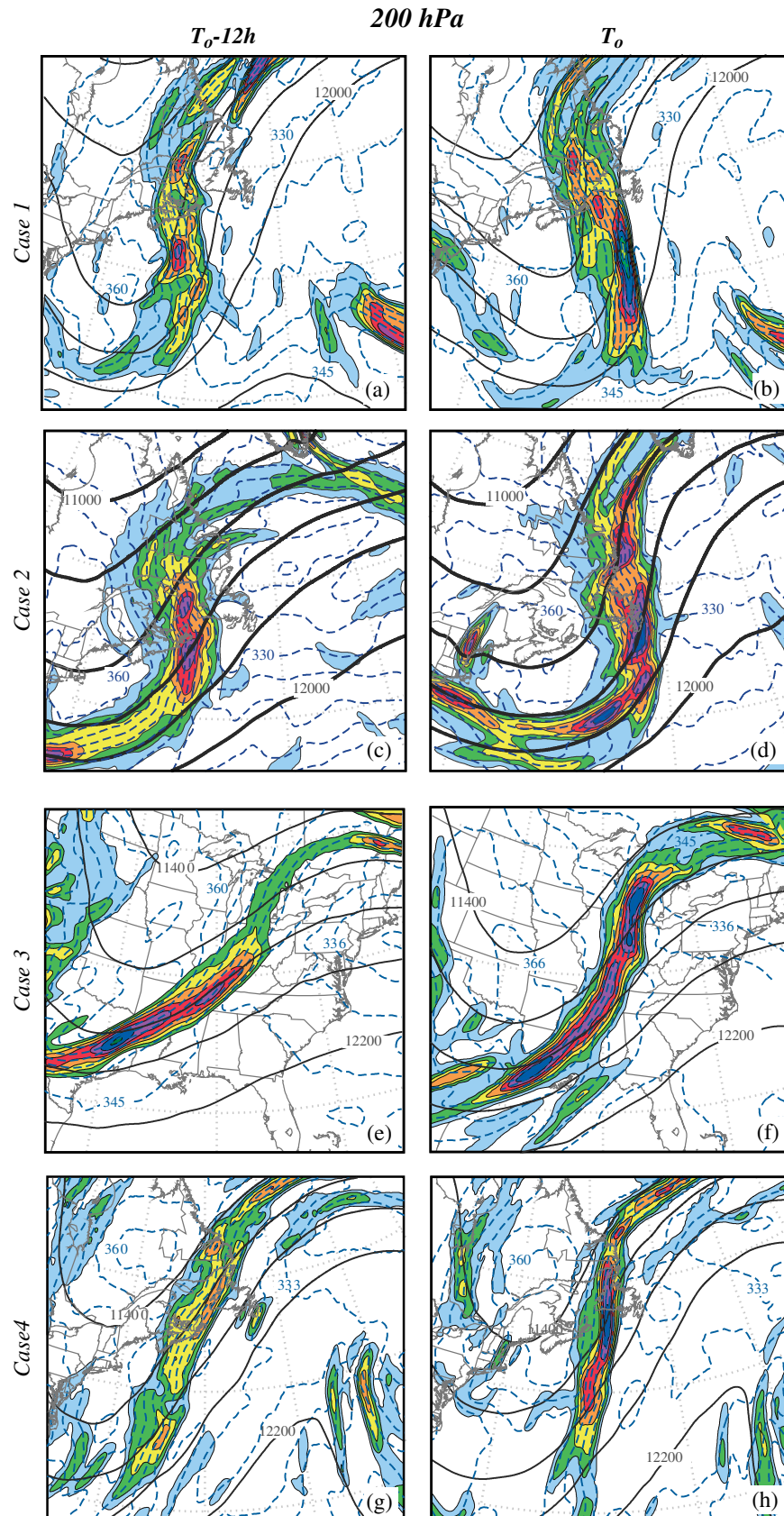


Figure 3. (a) 200 hPa geopotential height, θ , and $|\nabla\theta|$ from the GFS analysis valid at 1800 UTC 19 November 2008. Geopotential height (solid) is labelled in metres and contoured every 200 m. θ (dashed) is labelled in kelvins and contoured every 3K. $|\nabla\theta|$ is labelled in units of $\text{K} (100 \text{ km})^{-1}$ and shaded every $1 \text{ K} (100 \text{ km})^{-1}$ beginning at $2 \text{ K} (100 \text{ km})^{-1}$. (b) As in (a) but from the GFS analysis valid at 0600 UTC 20 November 2008. (c) As in (a) but from the GFS analysis valid at 0000 UTC 8 December 2008. (d) As in (a) but from the GFS analysis valid at 1200 UTC 8 December 2008. (e) As in (a) but from the GFS analysis valid at 0600 UTC 7 January 2009. (f) As in (a) but from the GFS analysis valid at 1800 UTC 7 January 2009. (g) As in (a) but from the GFS analysis valid at 0600 UTC 4 March 2009. (h) As in (a) but from the GFS analysis valid at 1800 UTC 4 March 2009.

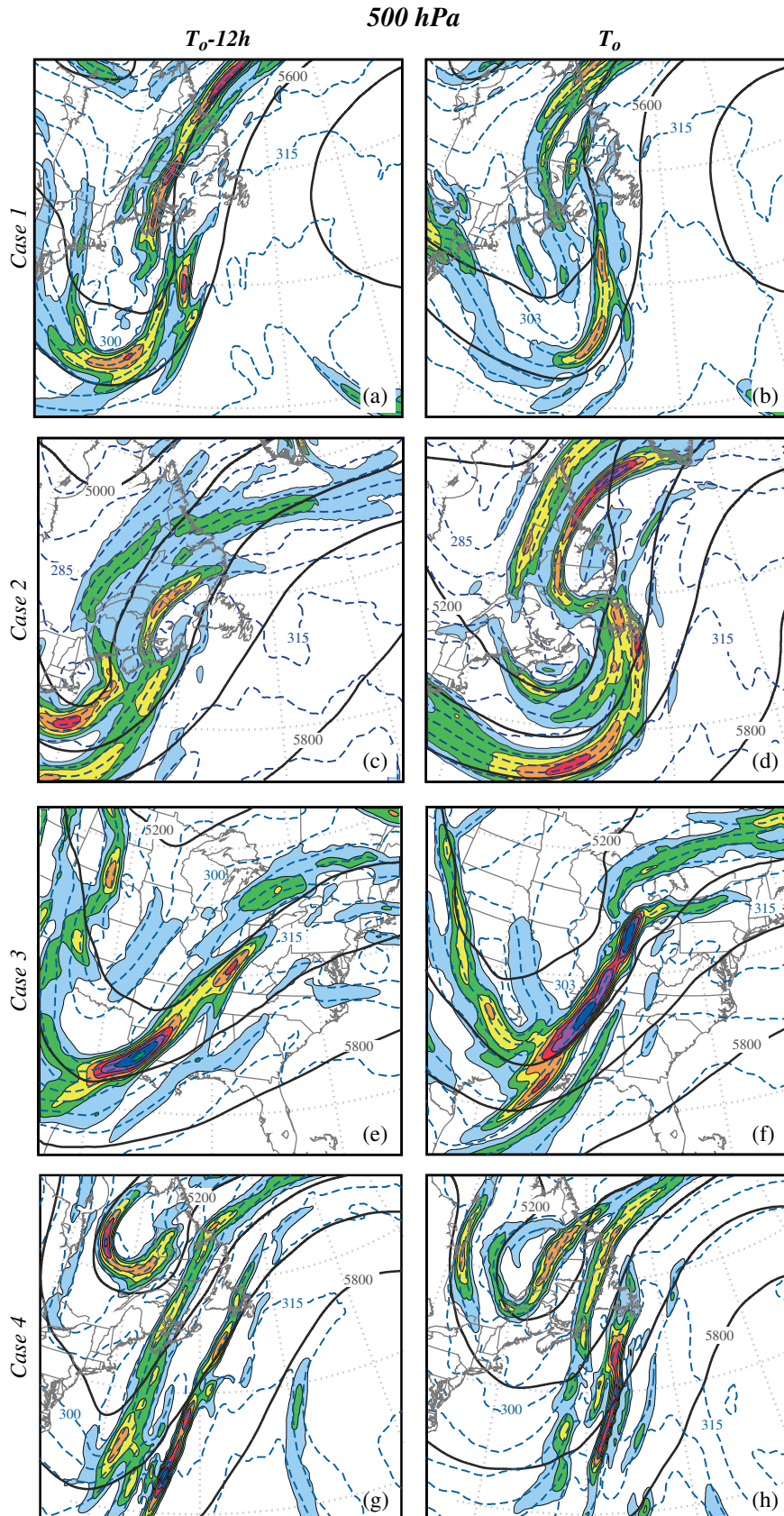


Figure 4. (a) 500 hPa geopotential height, θ , and $|\nabla\theta|$ from the GFS analysis valid at 1800 UTC 19 November 2008. Geopotential height (solid) is labelled in metres and contoured every 200 m. θ (dashed) is labelled in kelvins and contoured every 3 K. $|\nabla\theta|$ is labelled in units of $\text{K} (100 \text{ km})^{-1}$ and shaded every $1 \text{ K} (100 \text{ km})^{-1}$ beginning at $2 \text{ K} (100 \text{ km})^{-1}$. (b) As in (a) but from the GFS analysis valid at 0600 UTC 20 November 2008. (c) As in (a) but from the GFS analysis valid at 0000 UTC 8 December 2008. (d) As in (a) but from the GFS analysis valid at 1200 UTC 8 December 2008. (e) As in (a) but from the GFS analysis valid at 0600 UTC 7 January 2009. (f) As in (a) but from the GFS analysis valid at 1800 UTC 7 January 2009. (g) As in (a) but from the GFS analysis valid at 0600 UTC 4 March 2009. (h) As in (a) but from the GFS analysis valid at 1800 UTC 4 March 2009.

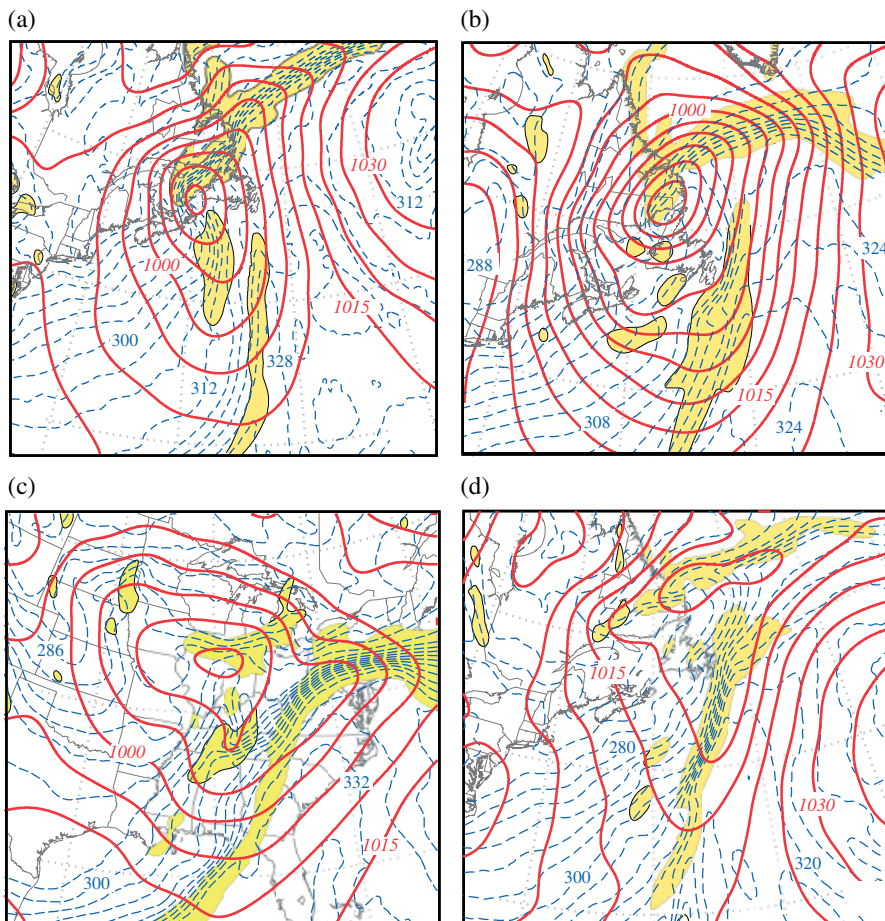


Figure 5. (a) Sea-level isobars (solid), 950 hPa θ_e (dashed) and 950 hPa horizontal frontogenesis (shaded) from the GFS analysis valid at 0600 UTC 20 November 2008. Isobars labelled in hectopascals and contoured every 5 hPa. 950 hPa θ_e labelled in kelvins and contoured every 4 K. Shading indicates 950 hPa horizontal frontogenesis exceeding $5 \text{ K (100 km)}^{-1} 3 \text{ h}^{-1}$. (b) As in (a) but from the GFS analysis valid at 1200 UTC 8 December 2008. (c) As in (a) but from the GFS analysis valid at 1800 UTC 7 January 2009. (d) As in (a) but from the GFS analysis valid at 1800 UTC 4 March 2009.

(Figure 5(b) and (c), respectively) were reminiscent of the T-bone frontal structure of the Shapiro and Keyser (1990) cyclone model. Within the southerly flow in the warm sector of these surface cyclones, moisture-laden air ($\theta_e > 320 \text{ K}$) was advected into the vicinity of the frontogenetically active cold front. In each case, the lower tropospheric frontogenesis was positioned slightly east of and parallel to the location of the 200 hPa lower stratospheric front (Figure 3).

3. Analysis I: Overview of common dynamical processes

With the focus on connecting the lower tropospheric and lower stratospheric frontogenesis processes, this section highlights the common dynamical mechanisms that promoted the development of each of the robust lower stratospheric fronts presented in section 2. The final time period (T_o) highlighted in the section 2 overview will be the focus of this analysis.

3.1. Diabatic stability tendency

In the Part I analysis, the southwesterly flow lower stratospheric frontogenesis process was dependent upon the magnitude of ascent in the cold upper troposphere, east of the lower stratospheric baroclinicity. Ascent in this region is a manifestation of the interplay between adjacent lower stratospheric forcing for ascent and the

local upper tropospheric stratification. The subsequent analysis highlights this linkage in the lower stratospheric frontogenesis process by quantifying the impact of latent heat release on the upper tropospheric thermal and static stability fields through the use of the static stability tendency equation, which can be written as

$$\frac{d}{dt} \left(-\frac{\partial \theta}{\partial p} \right) = \left(\frac{\partial}{\partial t} \vec{V} \cdot \nabla + \omega \frac{\partial}{\partial p} \right) \left(-\frac{\partial \theta}{\partial p} \right)$$

or

$$\frac{d}{dt} \left(-\frac{\partial \theta}{\partial p} \right) = -\frac{\partial}{\partial p} \left(\frac{d\theta}{dt} \right) - \frac{\partial \vec{V}}{\partial p} \cdot \nabla \theta - \frac{\partial \omega}{\partial p} \frac{\partial \theta}{\partial p}. \quad (1)$$

For each case, the rate of latent heating was obtained following the method employed by Emanuel *et al.* (1987)* and is calculated as

$$\frac{d\theta}{dt} = \dot{\theta} = \omega \left(\frac{\partial \theta}{\partial p} - \frac{\gamma_m}{\gamma_d} \frac{\theta}{\theta_e} \frac{\partial \theta_e}{\partial p} \right), \quad (2)$$

where $\dot{\theta}$ corresponds to latent heat release, ω is the vertical velocity (in Pa s^{-1}), and γ_d and γ_m are the dry and moist

*Emanuel *et al.* (1987) derived condensational heating in terms of moist and dry potential vorticity directly from the conservations of moist entropy in order to explore the effects of latent heat release on the development and structure of baroclinic waves.

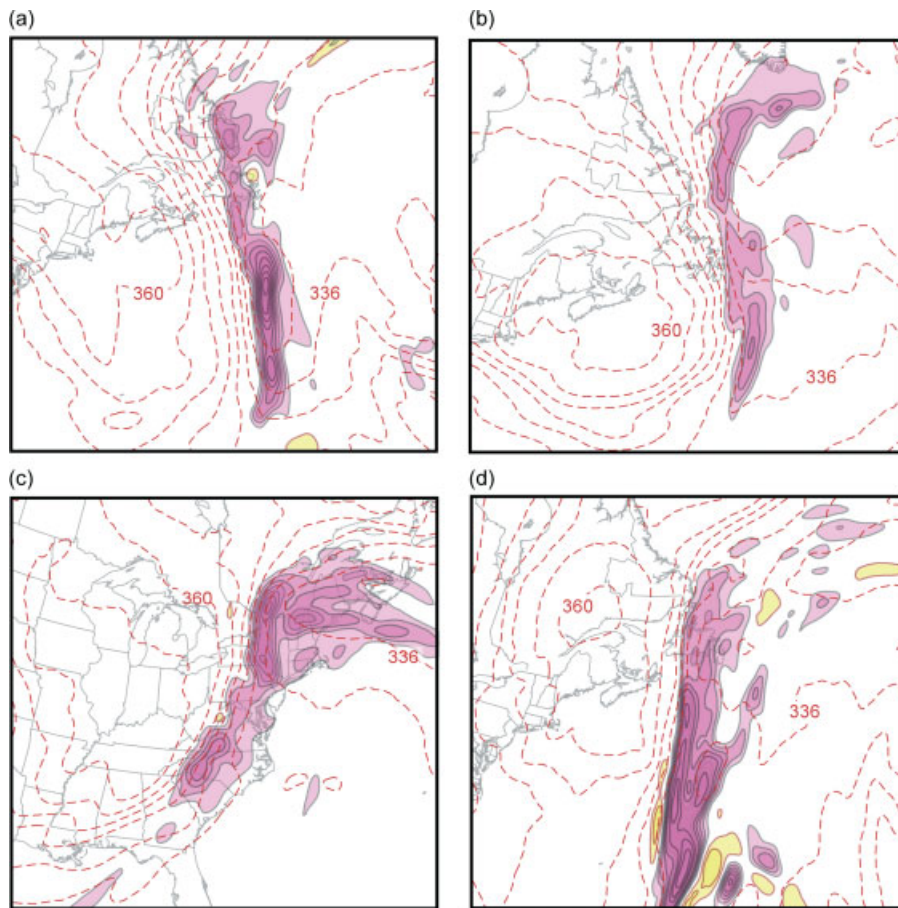


Figure 6. The 200 hPa potential temperature contoured every 4 K (dashed) and the diabatic static stability tendency at 250 hPa contoured every 1 K d^{-1} with purple (yellow) shading corresponding to a decrease (increase) in static stability. From the GFS analysis valid at (a) 0600 UTC 20 November 2008, (b) 1200 UTC 8 December 2008, (c) 1800 UTC 7 January 2009, and (d) 1800 UTC 4 March 2009.

adiabatic lapse rates, respectively. Using the thermal wind relationship and applying Eq. (2), Eq. (1) becomes

$$\frac{d}{dt} \left(-\frac{\partial \theta}{\partial p} \right) = \underbrace{-\frac{\partial \dot{\theta}}{\partial p}}_a - \underbrace{\frac{\partial \vec{V}_{\text{ag}}}{\partial p} \cdot \nabla \theta}_b - \underbrace{\frac{\partial \omega}{\partial p} \frac{\partial \theta}{\partial p}}_c, \quad (3)$$

where \vec{V}_{ag} is the ageostrophic component of the horizontal wind. The static stability tendency can be separated into three terms: term *a*, the diabatic static stability tendency; term *b*, the contribution from the tilting of horizontal temperature gradients into vertical temperature gradients (e.g. static stability) by the ageostrophic vertical shear; and term *c*, the contribution from the vertical stretching of isentropic layers. Together terms *b* and *c* represent the total contribution from the three-dimensional ageostrophic wind.

Focusing on the notion that lower tropospheric ascent can have a diabatic impact on the strength of the ascent in the vicinity of an ULJF, this section provides only an analysis of the diabatic contributions represented by term *a* in Eq. (3). At T_o , in each of these cases, terms *b* and *c* are roughly an order of magnitude smaller than term *a* and together contribute a small percentage to the overall static stability tendency field (not shown). Of course, in the vicinity of a straight ULJF, the configuration of the primary geostrophic flow is associated with the strength and structure of secondary ageostrophic Sawyer–Eliassen circulations. When applying Eq. (3) in the vicinity of relatively straight ULJFs, such as those presented in this

analysis, the contribution from terms *b* and *c* is directly related to the secondary Sawyer–Eliassen circulation. The nature of contributions to the static stability tendency that arise from the total forced secondary circulations in (3) (terms *b* and *c*) is left to future work.

In all four cases presented in section 2, the latent heat released in association with the lower tropospheric ascent allowed for a restructuring of the upper tropospheric static stability. The instantaneous diabatic static stability tendency, term *a* in Eq. (3), is calculated using the 10 min heating rates beginning at the given time. Figure 6 shows the distribution of this term at the 250 hPa level relative to the location of lower stratospheric (200 hPa) baroclinicity for each of the four cases. Each of the cases shows similar impacts from the diabatic processes associated with the tropospheric ascent. The latent heating weakened the upper tropospheric static stability in a linearly oriented band immediately to the cold (upper tropospheric) side of the lower stratospheric front. The location and orientation of the reduction in static stability was such that in each case it was located between the leading edge of both the lower stratospheric front and the lower tropospheric cold front. In the presence of forcing for vertical motion within the lower stratospheric frontal region, such a configuration of the static stability tendency would intensify the response to that forcing, particularly ascent on the cold side of the lower stratospheric front.

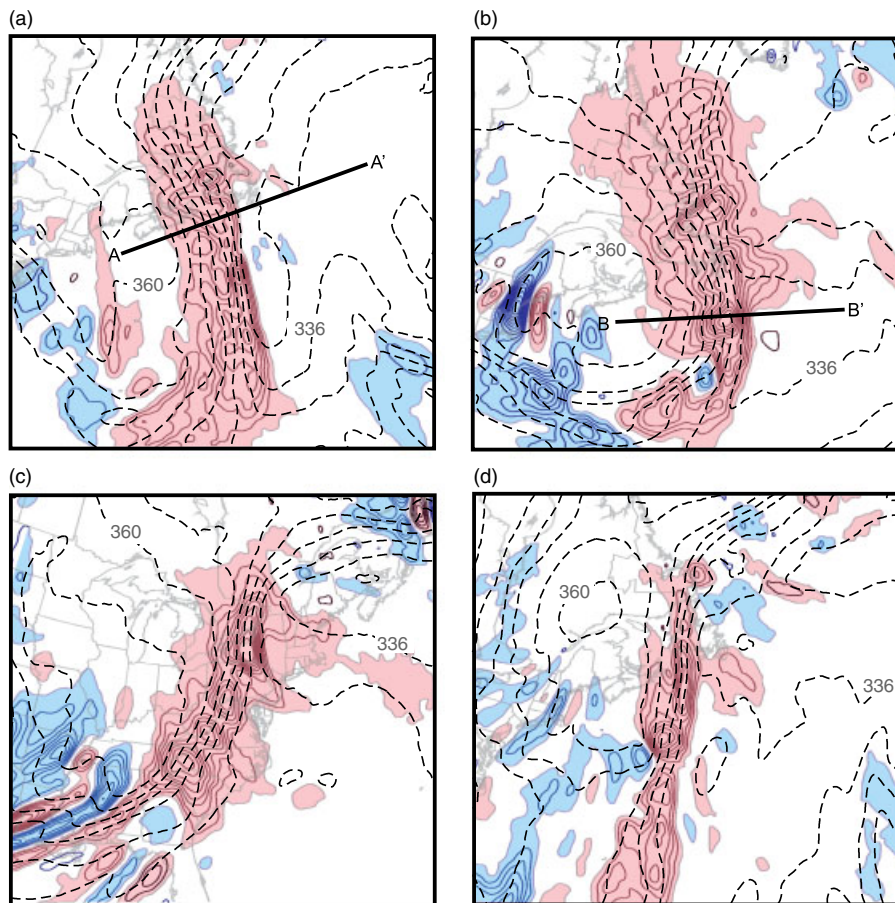


Figure 7. The 200 hPa potential temperature contoured every 4 K (dashed), the geostrophic isotachs every 10 m s^{-1} beginning at 40 m s^{-1} (solid), and the geostrophic temperature advection in pink (blue) shading above $3 \times 10^{-4} \text{ K s}^{-1}$ (below $-3 \times 10^{-4} \text{ K s}^{-1}$) and contoured every $3 \times 10^{-4} \text{ K s}^{-1}$. From the GFS analysis valid at (a) 0600 UTC 20 November 2008, (b) 1200 UTC 8 December 2008, (c) 1800 UTC 7 January 2009, and (d) 1800 UTC 4 March 2009.

3.2. Lower stratospheric QG forcing, ascent and tilting frontogenesis

Following the method employed in Part I, the analysis uses QG diagnostics, in the form of geostrophic temperature advection in cyclonic shear, to diagnose regions of vertical motion in the vicinity of the lower stratospheric front. To more precisely capture the dynamics involved in lower stratospheric frontogenesis, the tilting contribution to frontogenesis (F_{tilt}) at 200 hPa is calculated using the full model vertical motion from the GFS analyses, where

$$F_{\text{tilt}} = -\frac{1}{|\nabla\theta|} \left(\frac{\partial\theta}{\partial p} \left(\frac{\partial\omega}{\partial x} \frac{\partial\theta}{\partial x} + \frac{\partial\omega}{\partial y} \frac{\partial\theta}{\partial y} \right) \right). \quad (4)$$

The 200 hPa geostrophic temperature advection, at T_0 , for each of the cases is shown in Figure 7. In all four cases, a large elongated region of geostrophic warm air advection characterized the cyclonic shear side of the southwesterly flow. As conceptually illustrated by Figure 2(b), geostrophic warm air advection in the lower stratospheric cyclonic shear promotes QG ascent through the local jet core, in the cold upper troposphere. While the geostrophic warm air advection varied in magnitude along the jet in each case, a maximum greater than $\sim 27 \times 10^{-4} \text{ K s}^{-1}$ was common at the 200 hPa level in each of the cases. In addition, the cold side of each of the lower stratospheric fronts was adjacent to the diabatic reduction in static stability (shown

in Figure 6). With the geostrophic warm air advection in each case proximate to the regions of reduced static stability, an area of robust ascent on the cold side of the lower stratospheric front can be expected.

Coincident with the lower stratospheric geostrophic warm air advection (Figure 7) and the 250 hPa diabatic static stability reduction (Figure 6), the 200 hPa full model vertical motions reveal ascent oriented roughly linearly along the cold side of each of the lower stratospheric fronts (Figure 8). The strongest upward motion in each case was located directly to the east of the QG forcing, promoting adiabatic cooling on the cold side of the lower stratospheric front. The cooling response was particularly evident in Case 1, where at the 200 hPa level a narrow band of cold potential temperature was located in the regions of the maximum ascent along the lower stratospheric front (Figure 8(a)). Responding to the diabatic weakening of the static stability in the upper troposphere, the strong, forced upward vertical motion led to a period of notable lower stratospheric tilting frontogenesis in each case (Figure 9).

4. Analysis II: Vertical cross-sections

This section highlights aspects of the lower tropospheric and lower stratospheric coupling through the analysis of a vertical cross-section taken through the ULJF system in two of the four cases. The position of each cross-section was selected in order to fully illustrate the separate, yet

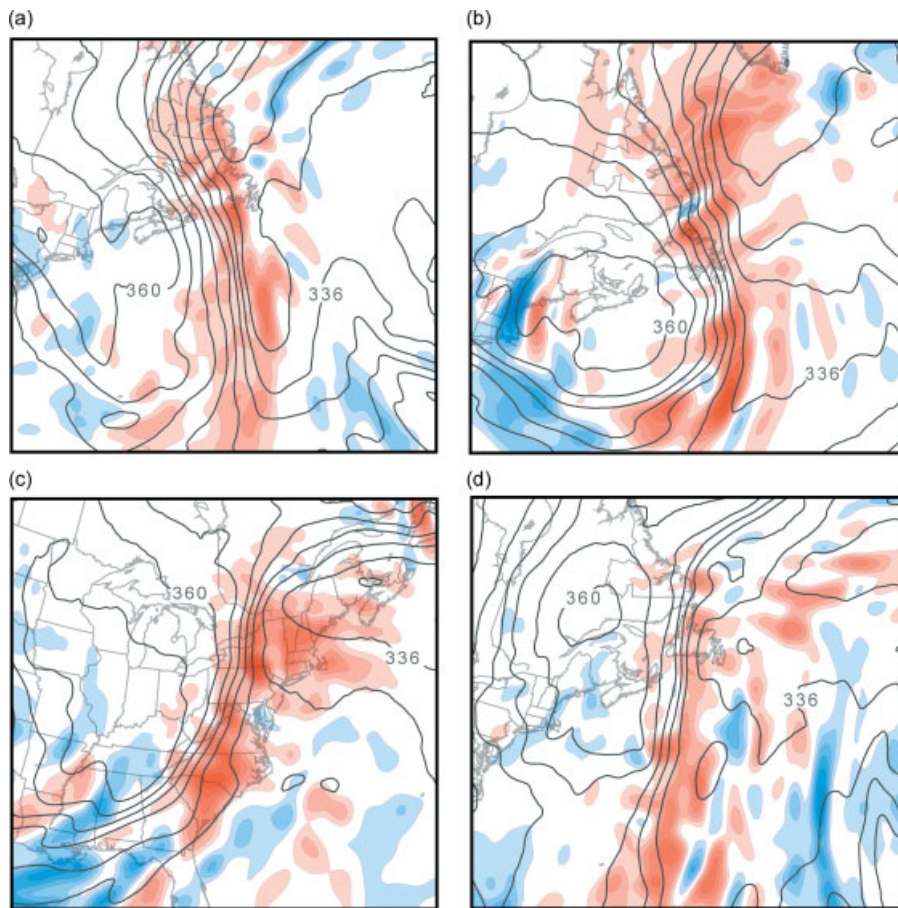


Figure 8. The 200 hPa potential temperature contoured every 4 K (solid) and vertical motion from the model analysis every 2 cm s^{-1} beginning at 2 cm s^{-1} in red (-2 cm s^{-1} in blue). From the GFS analysis valid at (a) 0600 UTC 20 November 2008, (b) 1200 UTC 8 December 2008, (c) 1800 UTC 7 January 2009, and (d) 1800 UTC 4 March 2009.

coupled, southwesterly-flow lower stratospheric and lower tropospheric processes at T_0 in Cases 1 and 2. The two cross-sections presented in this section are representative of all four cases and highlight the common coupling between the dynamical processes in the troposphere and lower stratosphere during lower stratospheric frontogenesis.

4.1. Case 1

A cross-section taken for Case 1 along the line A–A' in Figure 7(a) is shown in Figure 10. Below the level of maximum winds, the broad baroclinicity in the upper troposphere was characterized by weak geostrophic cold advection and associated subsidence. East of the location of the surface front was a vertical column of ascent (with a maximum of $>20 \text{ cm s}^{-1}$) that reached from the surface to roughly the 300 hPa level, just above the 324 K isentrope (roughly the value of the surface θ_e). The lower stratospheric cyclonic shear was characterized by a region of geostrophic warm air advection ($\sim 12 \times 10^{-4} \text{ K s}^{-1}$). Within the weak static stability on the cold side of the lower stratospheric front, but to the west of the lower tropospheric ascent, was a second column of ascent with a maximum in upward vertical motion greater than 15 cm s^{-1} centred at 250 hPa. This second column of ascent was associated with the geostrophic warm air advection that characterized the lower stratospheric front.

As in the southwesterly flow case presented in Part I, the near-tropopause upper tropospheric ascent maximum

(Figure 10) acted to increase the slope not only of the isentropes but also the tropopause, above the jet core (positive tilting frontogenesis). The diabatic static stability tendency associated with the distribution of latent heating shows a reduction in static stability directly above the lower tropospheric ascent (Figure 10). However, the region of reduced stability associated with latent heat release extends into the region directly to the cold side of the lower stratospheric front. The stability within this upper tropospheric region is important as it plays a role in determining the magnitude of the ascent responding to the QG forcing associated with the lower stratospheric front. Thus the distribution of latent heating in this case likely contributed to the development of robust ascent, associated with the lower stratospheric geostrophic warm air advection, by decreasing the stability in the near-tropopause upper troposphere. The strong ascent, located on the cold side of the lower stratospheric front, was well positioned to force a period of notable lower stratospheric frontogenesis via tilting.

4.2. Case 2

A cross-section taken for Case 2 along the line B–B' in Figure 7(b) is shown in Figure 11. Below the level of maximum winds, the troposphere was characterized by a region of weak geostrophic cold air advection. Immediately east of the location of the surface cold front, a column of ascent with a maximum in upward vertical motion greater

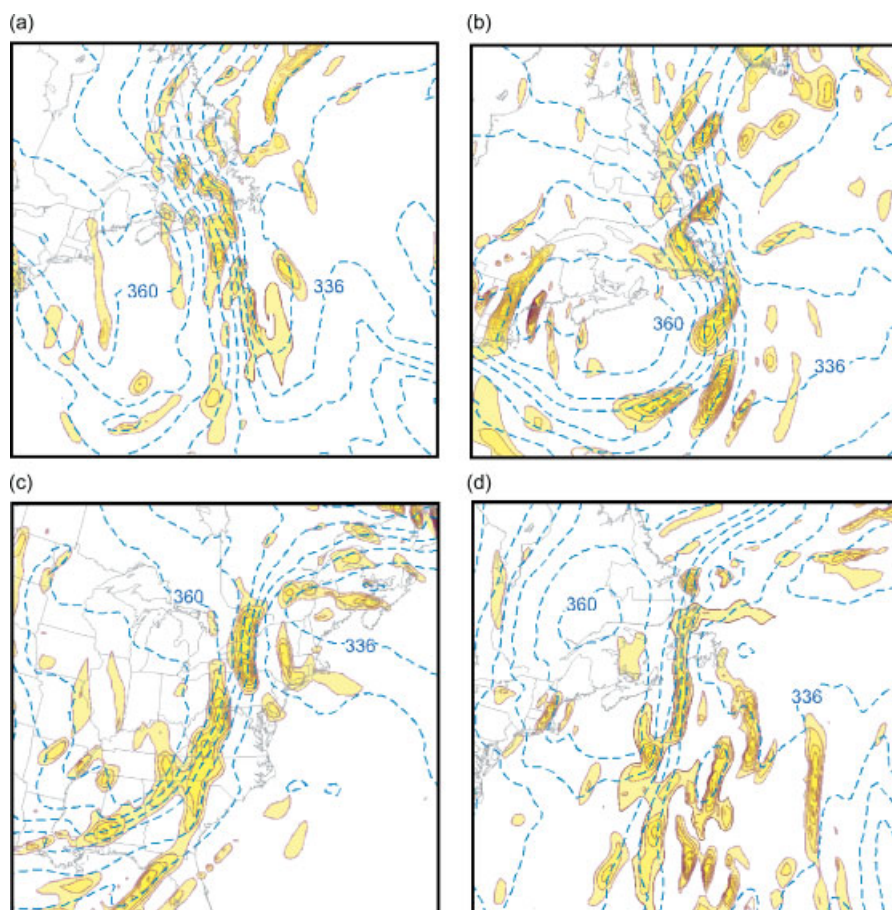


Figure 9. 200 hPa potential temperature contoured every 4 K (dashed) and positive tilting frontogenesis shaded and contoured every $4 \times 10^{-9} \text{ K m}^{-1} \text{ s}^{-1}$. From the GFS analysis valid at (a) 0600 UTC 20 November 2008, (b) 1200 UTC 8 December 2008, (c) 1800 UTC 7 January 2009, and (d) 1800 UTC 4 March 2009.

than 30 cm s^{-1} , reached from the surface to 250 hPa, the vicinity of the 328 K isentrope (approximately the θ_e at the surface). The lower stratospheric cyclonic shear was characterized by an intense region of geostrophic warm air advection ($> 33 \times 10^{-4} \text{ K s}^{-1}$). On the cold side of the lower stratospheric front and in the vicinity of the jet core was a second region of upward vertical motion (centred at ~ 250 hPa) with a maximum of $\sim 15 \text{ cm s}^{-1}$. As in Case 1, these two regions of ascent were associated with two separate diagnostic mechanisms: one in the form of lower tropospheric frontogenesis and the other in the form of lower stratosphere geostrophic warm air advection in cyclonic shear. The diabatic static stability tendency plotted at this time illustrates that the reduction in the static stability above the lower tropospheric ascent plume extended into the vicinity of the tropopause-level ascent plume. As the static stability in the near-tropopause upper troposphere was diabatically reduced, the strong lower stratospheric QG dynamics, in the form of geostrophic warm air advection in cyclonic shear, were coincident with the robust ascent and were tied to a period of lower stratospheric frontogenesis.

5. Summary and discussion

In an effort to investigate the connection between lower tropospheric ascent and the development of robust lower stratospheric fronts, four cases from the 2008–2009 winter were selected for diagnostic case study analysis. Although these four cases were selected based on the intensity of their

lower stratospheric fronts ($|\nabla\theta| > 8 \text{ K (100 km)}^{-1}$), each case was also associated with a lower tropospheric column of ascent forced by an active surface front. The accompanying surface front in each case was associated with a surface cyclone at the end of its life cycle and was located roughly parallel to and east of the position of the lower stratospheric front. By virtue of the near superposition of the surface and lower stratospheric fronts in the southwesterly flow cases, the analysis presented here illustrates that the diabatic impact of tropospheric frontal ascent (e.g. reduced upper tropospheric static stability) is consistently positioned so as to favour a robust response to lower stratospheric frontogenetic ascent on the cold side of the lower stratospheric frontal zone.

The results of this diagnostic analysis suggest a possible mechanism for a coupling between lower tropospheric and lower stratospheric processes, which is conceptually illustrated in Figure 12 and summarized below. As latent heat release associated with ascent along a surface frontal boundary reconfigures the potential temperature field (e.g. Emanuel *et al.*, 1987) within the upper troposphere, the static stability of the near-tropopause upper troposphere decreases. During the late stages of the mid-latitude cyclone life cycle when the lower tropospheric and lower stratospheric fronts are aligned, such a distribution of the diabatic static stability tendency can directly enhance the magnitude of the ascent on the cold side of the lower stratospheric front which is associated with geostrophic warm air advection in the lower stratospheric cyclonic shear. The resulting tilting subsequently contributes to the

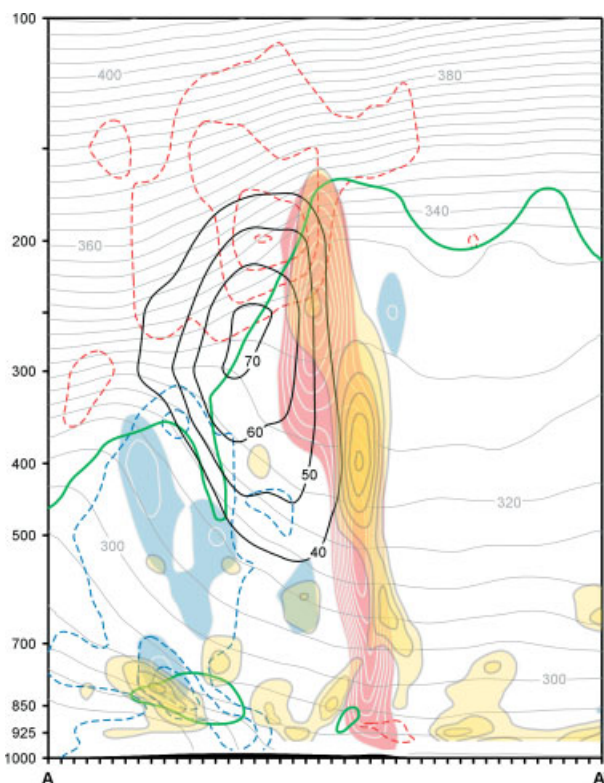


Figure 10. Vertical cross-section along the line A–A' in Figure 7(a) of potential temperature, geostrophic isotachs, geostrophic temperature advection, vertical motions and diabatic stability tendency from the GFS analysis valid at 0600 UTC 20 November 2008. Potential temperature (thin grey lines) is labelled in kelvins and contoured every 4 K. Geostrophic isotachs (thick black lines) labelled in m s^{-1} and contoured every 10 m s^{-1} beginning at 40 m s^{-1} . Vertical motion, with upward (downward) motion in the pink (blue) shading, is contoured every 2 cm s^{-1} beginning at $4 (-4) \text{ cm s}^{-1}$ then contoured every 5 cm s^{-1} after $20 (-20) \text{ cm s}^{-1}$. Geostrophic temperature advection (dashed lines) contoured every $3 \times 10^{-4} \text{ K s}^{-1}$ beginning at $3 (-3) \times 10^{-4} \text{ K s}^{-1}$ in red (blue). Negative diabatic static stability tendency contoured and shaded (yellow) every 1 K d^{-1} and beginning at -1 K d^{-1} .

intensification of a robust lower stratospheric front, and a steeper tropopause above the jet core.

Because of the diagnostic nature of the analysis employed here, it is not possible to definitively conclude that the reduction of upper tropospheric static stability via mid-level heating preceded the robust tilting frontogenesis near the tropopause. However, the circumstantial evidence in support of this sequence of events is strong since, upon considering the temporal evolution of each case (not shown), the lower stratospheric frontogenesis occurred only *after* each lower tropospheric front and its associated ascent became parallel to its lower stratospheric counterpart. Furthermore, a spatial coherency between the lower tropospheric ascent and the static stability tendency remained relatively constant from $T_0 - 12 \text{ h}$ to T_0 throughout the evolution of each case (not shown), suggesting that the region of reduced stability was a by-product of the surface frontal ascent.

The four cases analysed in this paper illustrate the possibility of several important synoptic–mesoscale dynamical links between lower tropospheric frontal processes and lower stratospheric dynamics. The analysis suggests that: (i) the impact of lower tropospheric frontal ascent on upper tropospheric static stability is likely able to influence the development of lower stratospheric fronts and

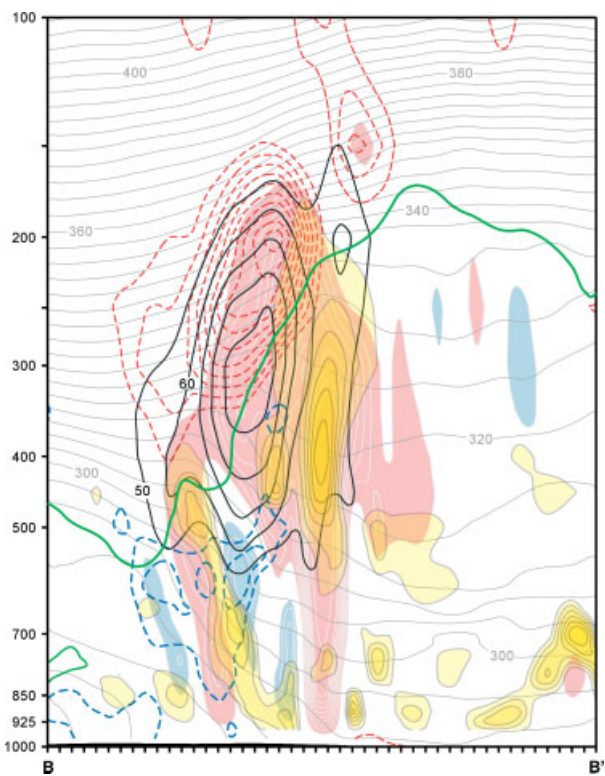


Figure 11. As Figure 10, but from the GFS analysis valid at 1200 UTC 8 December 2008 and along the line B–B' in Figure 7(b).

substantially alter the structure of a mid-latitude jet-front system by increasing the magnitude of ascent associated with lower stratospheric geostrophic warm air advection in cyclonic shear; (ii) an enhanced ascent maximum above the jet core can subsequently lead to an increase in the slope of not only the isentropes within the lower stratospheric front but also the tropopause above the jet core, via tilting; and (iii) when latent heat release occurs in the vicinity of a ULJF with a dynamically active lower stratospheric front, the lower stratospheric frontal circulation may be able to enhance the mesoscale structure of the horizontal PV gradient (i.e. increase the tropopause slope) above the jet core.

The analysis presented here highlights the interactions between lower stratospheric frontal development and the reduction of static stability produced by *in situ* moist processes along surface frontal zones. There are, of course, a variety of mechanisms whereby poorly stratified air may be delivered to or created within the upper troposphere to similarly influence lower stratospheric development. One such method may involve long-wave radiative cooling at and above the tropopause level; however, its role remains open to future investigation. Other methods are related to the type of tropospheric ascent. For example, the large-scale ascent present within warm conveyor belts, characterized by vertical displacements of more than 600 hPa within 2 days (Wernli and Davies, 1997), can diabatically alter the large-scale PV distribution of the upper troposphere (e.g. Wernli, 1997; Pomroy and Thorpe, 2000; Grams *et al.*, 2011) so as to work in concert with lower stratospheric frontal processes. The results presented here provide an additional perspective on the impact of WCB-related ascent and diabatic processes on the evolution of near tropopause features.

Alternatively, the outflow from organized convection – of either mid-latitude (e.g. squall lines or mesoscale convective

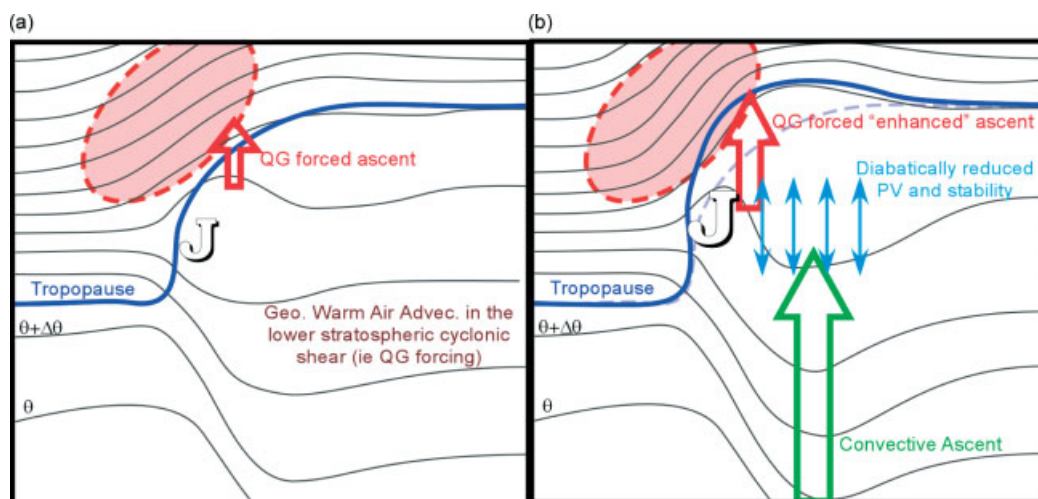


Figure 12. Conceptual model of the impact of convectively generated latent heat release on lower stratospheric frontal development as shown in idealized cross-sections through jet-front systems (a) without convection and (b) with convection. (a) A dynamically active lower stratospheric front, characterized by geostrophic warm air advection in cyclonic shear (pink shading), forces ascent (red arrow) that can increase the slope of the isentropes (thin lines) and dynamic tropopause (blue line) above the jet core via frontogenetic tilting. (b) Convectively generated latent heat release reduces the stability in the near-tropopause upper troposphere and can enhance the response to the lower stratospheric QG forcing (larger arrow), thereby intensifying the lower stratospheric tilting frontogenesis process, resulting in a more steeply sloped tropopause and an intensified tropopause jet. See text for explanation.

systems) or tropical origin (e.g. convective clusters, tropical plumes or tropical cyclones) – processes low-PV, low-static-stability, boundary layer air in convective updraughts and exhausts such air into the upper troposphere. If a pre-existing mid-latitude jet becomes juxtaposed with such outflow, the convective outflow may be linked to a period of lower stratospheric frontogenesis as well as changes in the slope of the tropopause above the jet core. Such changes, tied as they are to increases in lower stratospheric baroclinicity, must also be potential energy generating and thus may provide a means by which energy released in the convection might be stored for subsequent release downstream in space and time. A number of studies have recently highlighted a link between the convective tropical cyclone environment and associated changes in the structure of the mid-latitude jet (e.g. Harr and Elsberry, 2000; Harr *et al.*, 2000; Klein *et al.*, 2000, 2002; Kitabatake, 2002, 2008; Agusti-Panareda *et al.*, 2004), where such interactions have implications on the development of downstream high-impact weather and downstream predictability and ensemble model spread. It is suggested that the analysis presented here provides insight into one of the mechanisms that may facilitate the observed tropical cyclone–extratropical jet interaction. Whether or not such interactions routinely manifest themselves in lower stratospheric frontal development is a topic for future inquiry.

References

- Agusti-Panareda A, Thorncroft CD, Craig GC, Gray SL. 2004. The extratropical transition of hurricane Irene (1999): a potential-vorticity perspective. *Q. J. R. Meteorol. Soc.* **130**: 1047–1074.
- Eliassen A. 1962. On the vertical circulation in frontal zones. *Geof. Publ.* **24**: 147–160.
- Emanuel KA, Fantini M, Thorpe AJ. 1987. Baroclinic instability in an environment of small stability to slantwise moist convection. Part I: Two-dimensional models. *J. Atmos. Sci.* **44**: 1559–1573.
- Grams CM, Wernli H, Böttcher M, Campa J, Corsmeier U, Jones SC, Keller JH, Lenz C-J, Wiegand L. 2011. The key role of diabatic processes in modifying the upper-tropospheric wave guide: a North Atlantic case-study. *Q. J. R. Meteorol. Soc.* **137**: 2174–2193.
- Harr PA, Elsberry RL. 2000. Extratropical transition of tropical cyclones over the western north Pacific. Part I: Evolution of structural characteristics during the transition process. *Mon. Weather Rev.* **128**: 2613–2633.
- Harr P, Elsberry RL, Hogan T. 2000. Extratropical transition of tropical cyclones over the western North Pacific. Part II: The impact of midlatitude circulation characteristics. *Mon. Weather Rev.* **128**: 2634–2653.
- Keyser D, Shapiro MA. 1986. A review of the structure and dynamics of upper-level frontal zones. *Mon. Weather Rev.* **114**: 452–499.
- Kitabatake N. 2002. Extratropical transformation of Typhoon Vicki (1987): structural change and the role of upper-tropospheric disturbances. *J. Meteorol. Soc. Jpn.* **80**: 229–247.
- Kitabatake N. 2008. Extratropical transition of tropical cyclones in the western North Pacific: their frontal evolution. *Mon. Weather Rev.* **136**: 2066–2090.
- Klein PM, Harr PA, Elsberry RL. 2000. Extratropical transition of western North Pacific tropical cyclones: an overview and conceptual model of the transformation stage. *Weather Forecast.* **15**: 373–396.
- Klein PM, Harr PA, Elsberry RL. 2002. Extratropical transition of western North Pacific tropical cyclones: midlatitude and tropical cyclone contributions to reintensification. *Mon. Weather Rev.* **130**: 2240–2259.
- Lang AA, Martin JE. 2012. The structure and evolution of lower stratospheric frontal zones. Part I: Examples in northwesterly and southwesterly flow. *Q. J. R. Meteorol. Soc.* **138**: 1350–1365.
- Pomroy HR, Thorpe AJ. 2000. The evolution and dynamical role of reduced upper-tropospheric potential vorticity in intensive observing period one of FASTEX. *Mon. Weather Rev.* **128**: 1817–1834.
- Rotunno R, Skamarock WC, Sayder C. 1994. An analysis of frontogenesis in south-westerly and north-westerly flow. *J. Atmos. Sci.* **51**: 3373–3398.
- Sawyer JS. 1956. Vertical circulation at meteorological fronts and its relation to frontogenesis. *Proc. R. Soc.* **A234**: 346–362.
- Schultz DM, Doswell CA. 1999. Conceptual models of upper-level frontogenesis in south-westerly and north-westerly flow. *Q. J. R. Meteorol. Soc.* **125**: 2535–2562.
- Shapiro MA. 1982. Mesoscale Weather Systems of the Central United States. 78 pp. CIRES University of Colorado/NOAA: Boulder, CO.
- Shapiro MA, Keyser D. 1990. Fronts, jet streams and the tropopause. In *Extratropical Cyclones: The Erik Palmén Memorial Volume*, Newton CW, Holopainen EO (eds). American Meteorological Society: Boston, MA; 167–191.
- Wernli H, Davies HC. 1997. A Lagrangian-based analysis of extratropical cyclones. I: The Methods and some applications. *Q. J. R. Meteorol. Soc.* **123**: 467–489.
- Wernli H. 1997. A Lagrangian-based analysis of extratropical cyclones. II: A detailed case-study. *Q. J. R. Meteorol. Soc.* **123**: 1677–1706.